ACS OMEGA

http://pubs.acs.org/journal/acsodf

Article

Improving Anticancer Activity of Chrysin using Tumor Microenvironment pH-Responsive and Self-Assembled Nanoparticles

Ashok Kumar Jangid, Raghu Solanki, Sunita Patel, Kanakaraju Medicherla, Deep Pooja,* and Hitesh Kulhari*

Cite This: *ACS Omega* 2022, 7, 15919−15928

Read Online

ACCESS | Metrics & More | Article Recommendations | Supporting Information

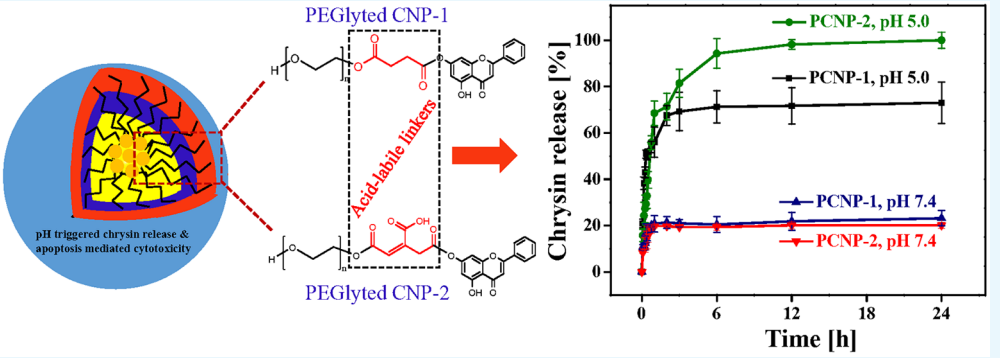

ABSTRACT: Chrysin is a natural bioactive compound with potential biological activities. However, unfavorable physicochemical properties of native chrysin make it difficult to achieve good therapeutic efficacies. In this study, poly(ethylene) glycol (PEG_{4000})-conjugated chrysin nanoparticles were prepared. The PEG_{4000} was conjugated to chrysin through *cis*-aconityl and succinoyl linkers to achieve tumor microenvironment-specific drug release from PEGylated nanoparticles. The conjugation of PEG and chrysin via succinoyl (PCNP-1) and *cis*-aconityl (PCNP-2) linkers was confirmed by the ^{1}H NMR and FTIR analysis. The nanoparticles were characterized by DLS, TEM, XRD, and DSC analysis. Comparatively, PCNP-2 showed a better drug release profile and higher anticancer activity against human breast cancer cells than chrysin or PCNP-1. The apoptosis studies and colony formation inhibition assay revealed that the PCNP-2 induced more apoptosis and more greatly controlled the growth of human breast cancer cells than pure chrysin. Thus, the use of PCNPs may help to overcome the issues of chrysin and could be a better therapeutic approach.

1. INTRODUCTION

In the 21st century, phytoconstituents have emerged as the most prominent source of many anticancer agents and represent an alternative to synthetic chemotherapeutic agents for cancer treatment.[1] A wide range of phytoconstituents, particularly bioflavonoids, have shown potential anticancer activities against various cancers. Chrysin (5,7-dihydroxy-2-phenyl-4*H*-chromen-4-one) is one such natural, plant-based bioflavonoid with broad-spectrum anticancer activity.[2] This molecule is extracted from *Passiflora caerulae*, *Passiflora incarnata*, honey, propolis, and honeycombs.[3] The preclinical studies of chrysin have shown its potential anticancer effects through selective cell signaling mechanisms, which are connected to cell proliferation, inflammation, angiogenesis, and cancer metathesis.[4−6] Chrysin was found to be effective against various cancers including breast, lung, bladder, thyroid, prostate, colon, etc.[2,5,7−9]

Despite the potential efficacy of chrysin in cancer treatment, some major challenges hinder the clinical use of chrysin. These challenges are low aqueous solubility (3 μg/mL), poor cellular uptake, physiochemical instability, rapid metabolism, and low oral bioavailability.[10,11] Therefore, in the past few years, many attempts have been made to improve the physicochemical properties and delivery of chrysin. Researchers have used micronization,[12] nanoemulsion, nanomicelles, nanosuspension, host−guest complexes, different derivatization, and salt formation approaches.[13−17] However, these systems still have a few drawbacks and cannot deliver the drug site-specifically. Therefore, inspired by the specific tumor microenvironment, we have developed self-assembled nanoparticles of chrysin by conjugating it with PEG_{4000} via acid-sensitive linkers. Further,

Received: February 21, 2022
Accepted: April 13, 2022
Published: April 25, 2022

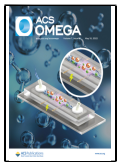

it is reported that the drug−polymer conjugated system shows high drug loading and enhanced therapeutic efficacy in comparison to the physical encapsulation of the drug-loaded system.[18] In a study, chrysin-loaded PLGA−PEG nanoparticles were also prepared and used against T47D (IC_{50} = 31.28 μM) and MCF7 (IC_{50} = 52.54 μM) breast cancer cells[19] and gastric cancer AGS cell (IC_{50} = 36.8 μM) lines.[20] In another interesting study, $PEG_{1K/2K}$-chrysin conjugate was developed for the delivery of doxorubicin where the directly conjugated chrysin did not show any sign of toxicity against the HepG2 cells.[21]

PEG is an FDA-approved, hydrophilic polymer and is generally used as an excipient in different pharmaceutical formulations.[22−25] High biocompatibility and hydrophilic nature make PEG an attractive polymer for formulation development.[26] PEGylation of hydrophobic drugs improves their aqueous solubility, improves cellular uptake, prolongs circulation in the blood and therefore *in vivo* performance, and improves overall therapeutic efficacy.[27−31] The development of a pH-responsive system helps in the site-specific delivery of therapeutic agents, particularly in cancer chemotherapy. The pH of the tumor microenvironment (pH 6.5−6.8) is slightly acidic as compared with physiological pH 7.4. This pH difference provides an opportunity for selective delivery of drugs using pH-sensitive drug carriers.[32−34] Herein, we have conjugated chrysin to PEG using two pH-sensitive linkers, i.e., succinoyl and *cis*-aconityl, and evaluated its anticancer activity. The synthesized system was able to self-assemble at the nanoscale, which was characterized by different analytical techniques.

2. EXPERIMENTAL SECTION

2.1. Materials. Chrysin (CHRY), 4-dimethylaminopyridine (DMAP), *cis*-aconitic anhydride (CAA), 1-ethyl-3-(3-(dimethylamino)propyl) carbodiimide (EDC), hydroxybenzotriazole (HOBt), fetal bovine serum (FBS), dimethyl sulfoxide (DMSO), phosphate buffer saline (PBS), dialysis tubing (molecular weight cut off 2 kDa), acridine orange, and ethidium bromide were obtained from Sigma-Aldrich (St. Louis, MO, USA). 3-(4,5-Dimethylthiahiazol-2-yl)-2,5-diphenyltetrazolium bromide (MTT), Minimum Essential Medium (MEM) and Dulbecco's Modified Eagle's Medium (DMEM) were purchased from HiMedia Laboratories (Mumbai, India). Succinic anhydride (SA), triethylamine, diethyl ether, glacial acetic acid, and dichloromethane were purchased from Rankem (Mumbai, India).

2.2. Synthesis of pH-Sensitive PEGylated Chrysin Conjugate. The PEGylated chrysin conjugates were synthesized by a two-step reaction. First, the hydroxyl group of PEG_{4000} was modified into succinoyl and *cis*-aconityl functionals using succinic anhydride and *cis*-aconitic anhydride, respectively.[35] In the next step, after 6 h of stirring, a solution of modified PEG_{4000} (mPEG, 0.500 g, 0.12 mmol), EDC (0.285 g, 0.18 mmol), and NHS (0.07 g, 0.06 mmol) in DMSO was dropwise added to the solution of chrysin (0.30 g, 0.12 mmol) in DMSO. The mixture was stirred for 24 h under nitrogen conditions. The resulting solution was dialyzed (MWCO 2 kDa) against ultrapure Milli-Q water, with the water changed every 6 h cycle, up to 3 days, and the product was collected by lyophilization.

2.3. Characterization of PEGylated Chrysin Conjugates. The PEGylated chrysin conjugates were characterized by proton nuclear magnetic resonance (Bruker 500-MHz Ultra shield plus NMR instrument) and Fourier transform infrared (PerkinElmer Spectrum 65 series, USA) spectroscopic techniques. For the NMR analysis, the PEGylated chrysin conjugates were dissolved in $CDCl_3$, and pure chrysin was dissolved in DMSO-d_6 solvent. Then both were scanned using a ^{1}H NMR (500 MHz) instrument. For the FTIR analysis, samples were mixed with KBr, pelletized, and scanned from 4000 to 400 cm^{-1}. The critical aggregation concentrations of the conjugates were measured using the pyrene fluorescent method, as previously reported.[36] A 25 μL aliquot of pyrene solution (6×10^7 M) was incubated with 5−500 μg/mL of PEGylated chrysin conjugates in the dark and at room temperature for 3 h. After that, samples were used to measure fluorescence intensities at a 339 nm excitation and 383 and 373 nm emission intensities. The fluorescence intensities were measured using a microplate reader (Synergy H1 Hybrid Reader, Biotek; Winooski, VT, USA). The intensity ratio and concentration of PEGylated chrysin conjugates were plotted to determine the critical micelle concentration (CMC) value.

2.4. Preparation of PEGylated Chrysin Nanoparticles (PCNP). To obtain PEGylated chrysin nanoparticles, i.e., PCNP-1 (PEG_{4000}−chrysin via succinoyl linker) and PCNP-2 (PEG_{4000}−chrysin via *cis*-aconityl linker), the conjugates were dissolved in acetone at a concentration of 10 mg/mL. Then, 3 mL of this solution was dropwise added to 15 mL of water under stirring at 1000 rpm. After that, the mixtures were kept stirring (1000 rpm, RT) for 3 h to evaporate acetone. The chrysin content in nanoparticles was quantified by a UV−visible spectrophotometer at 266 nm, and % drug content was calculated by the following equation.

$$\text{chrysin content (\%)} = \left[\frac{\text{amount of chrysin in PCNPs}}{\text{total weight of PEG}_{4000} - \text{chrysin conjugate}}\right] \times 100$$

2.5. Characterizations of PCNP. The size distribution of PCNP-1 and PCNP-2 was determined using DLS technique (Malvern Instruments, UK). TEM instrument (JEOL JEM-2100 TEM, Tokyo, Japan) was used to confirm the morphology of nanoparticles. Powder XRD (D8 Advance, Bruker, Germany) and DSC (DSC 4000, PerkinElmer, USA) instruments were used to confirm the physical state of the prepared nanoparticles.[35]

2.6. *In Vitro* Drug Release Study. The release of chrysin from PCNP-1 and PCNP-2 was performed using the dialysis method.[37] PCNP-1 and PCNP-2 nanoparticles were separately placed in a dialysis bag (MWCO 2 kDa). The formulation-containing dialysis bag was immersed in 100 mL of sodium acetate buffer (pH 5.0), phosphate buffer (pH 6.5), or phosphate buffer saline (pH 7.4). The experiment was performed at 37 °C and with 100 rpm stirring speed. At different intervals, aliquots from the released media were collected for drug analysis and replenished with an equivalent volume of fresh media.

2.7. Stability Study. The stability study of prepared PCNPs was performed by measuring particle size (colloidal stability) and % drug content (drug stability) over a period of 96 h at refrigeration temperature. The change in particle size was measured by DLS method, and % chrysin content was measured using a UV−visible spectroscopic method.

2.8. Cell Culture. Human breast cancer (MDA-MB-231) and MCF-7 cells were purchased from NCCS (Pune, India) and cultured in Dulbecco's Modified Eagle's Medium-high

https://doi.org/10.1021/acsomega.2c01041
ACS Omega 2022, 7, 15919−15928

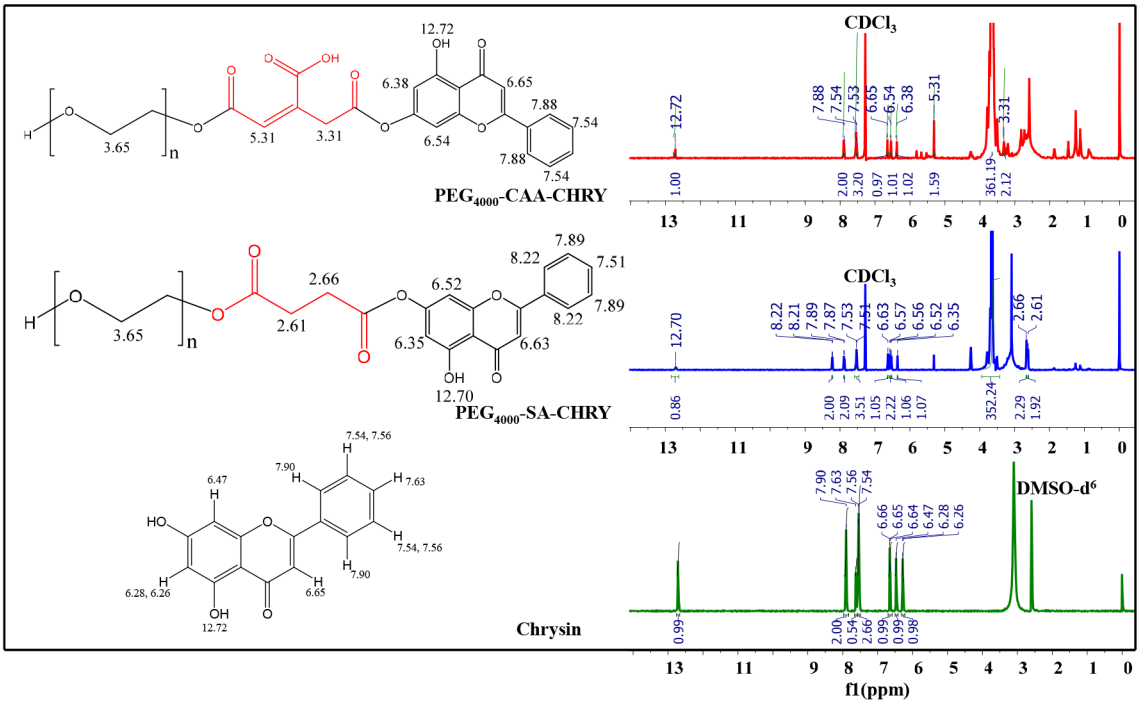

Figure 1. ^{1}H NMR spectra of chrysin, PEG_{4000}−chrysin via succinoyl linker (PEG_{4000}−SA−CHRY), and PEG_{4000}−chrysin via *cis*-aconityl linker (PEG_{4000}−CAA−CHRY).

Glucose (DMEM-HG) and MEM, respectively, with 10% fetal bovine serum (FBS) in a fully humidified atmosphere of 5% CO_2 at 37 °C. After reaching 80% to 90% confluency, cells were trypsinized for experiments.[38]

2.8.1. In Vitro Cytotoxicity Assay. To evaluate the anticancer activity of prepared nanoparticles, an *in vitro* cytotoxicity assay was performed. About 7.0 × 10^3 cells/well were seeded in 96-well plates and incubated for 24 h in a CO_2 incubator. After that, cells were treated with pure chrysin, PCNP-1, and PCNP-2 at different concentrations (5, 10, 20, 40, 60, 80, and 100 μg/mL). After the completion of the incubation period (24 and 48 h), media from the wells was discarded, and fresh media containing 0.5 mg/mL of MTT reagent was added to each well. After 4 h of incubation, MTT solution was removed, and crystal formazan was dissolved by adding 100 μL of DMSO to each well. After 10 min of incubation, absorbance was measured at 570 nm using a multimode plate reader (Synergy H1, Biotek, USA). Untreated cells were considered as a control, and % cell viability was determined with respect to the viability of the control cells.

2.8.2. Apoptotic Assay. To examine the cellular changes after treatment with PCNP, an apoptotic assay was performed by acridine orange/ethidium bromide (AO/EtBr) staining, as previously reported.[38] About 4.0 × 10^4 cells/well were seeded in 12-well plates. After 24 h, the cells were treated with pure chrysin, PCNP-1 and PCNP-2, equivalent to 10 μg/mL of chrysin. After the completion of the incubation period (24 and 48 h), the cells were trypsinized and centrifuged at 1800 rpm for 5 min. The resultant cell pellets were dispersed in 1× PBS, and 10 μL of suspension was taken for further examination. The cell suspension was mixed with 5 μL of AO dye (1 mg/mL) and EtBr dye (1 mg/mL) and mounted on a clean glass slide. Then, cells were observed using a fluorescence microscope (Zeiss, Germany). The cells were counted using ImageJ software and plotted as % cells in a stacked column graph by using Graphpad Prism 6.

2.8.3. Colony Formation Assay. To assess the colony formation potential of MDA-MB-231 cells after the treatment with PCNP, a colony formation assay was performed.[39] For that, about 300 cells/well were seeded in 6-well plates. After 24 h, cells were treated with a concentration of 10 μg/mL of pure chrysin, PCNP-1, and PCNP-2. The plates were kept in a CO_2 incubator for 7 days to allow the cells to form colonies. Further, the media was discarded and washed twice with 1× PBS. The cells were fixed with cell-fixing solution (95:5, ethanol and glacial acetic acid) for 15 min. The cell-fixing solution was removed, and the cells were washed with PBS. Finally, the colonies were stained by crystal violet staining solution (5 mg/mL crystal violet in 2% ethanol) for 15 min at room temperature and washed with PBS. The number of colonies were counted under microscope (Carl Zeiss, Germany), and a graph was plotted by using GraphPad Prism software (GraphPad 6.0). Representative images were taken by a digital camera (Nikon 1000D camera, Taiwan).

2.8.4. Cellular Uptake Study. To evaluate the internalization of PCNP into MDA-MB-231 cells, a cellular uptake study was performed, as previously reported.[40] For that, coumarin-6 (C6) was used as a fluorescence probe and encapsulated in PCNP-1 (C6-CNP-1) and PCNP-2 (C6-CNP-1). About 2.0 × 10^4 cells/well were seeded into 35 mM cell culture dishes and allowed to incubate for 24 h. Further, cells were treated with 50 μg/mL concentration of C6-CNP-1 and C6-CNP-2 for 0, 0.5, 1, 2, 4, and 8 h. At the different time intervals, plates were washed twice with PBS and observed under a fluorescence microscope (Zeiss Axio Scope A1, Germany).

2.9. Statistical Analysis. All the experimental measurements were performed in triplicate, and the values are

https://doi.org/10.1021/acsomega.2c01041
ACS Omega 2022, 7, 15919−15928

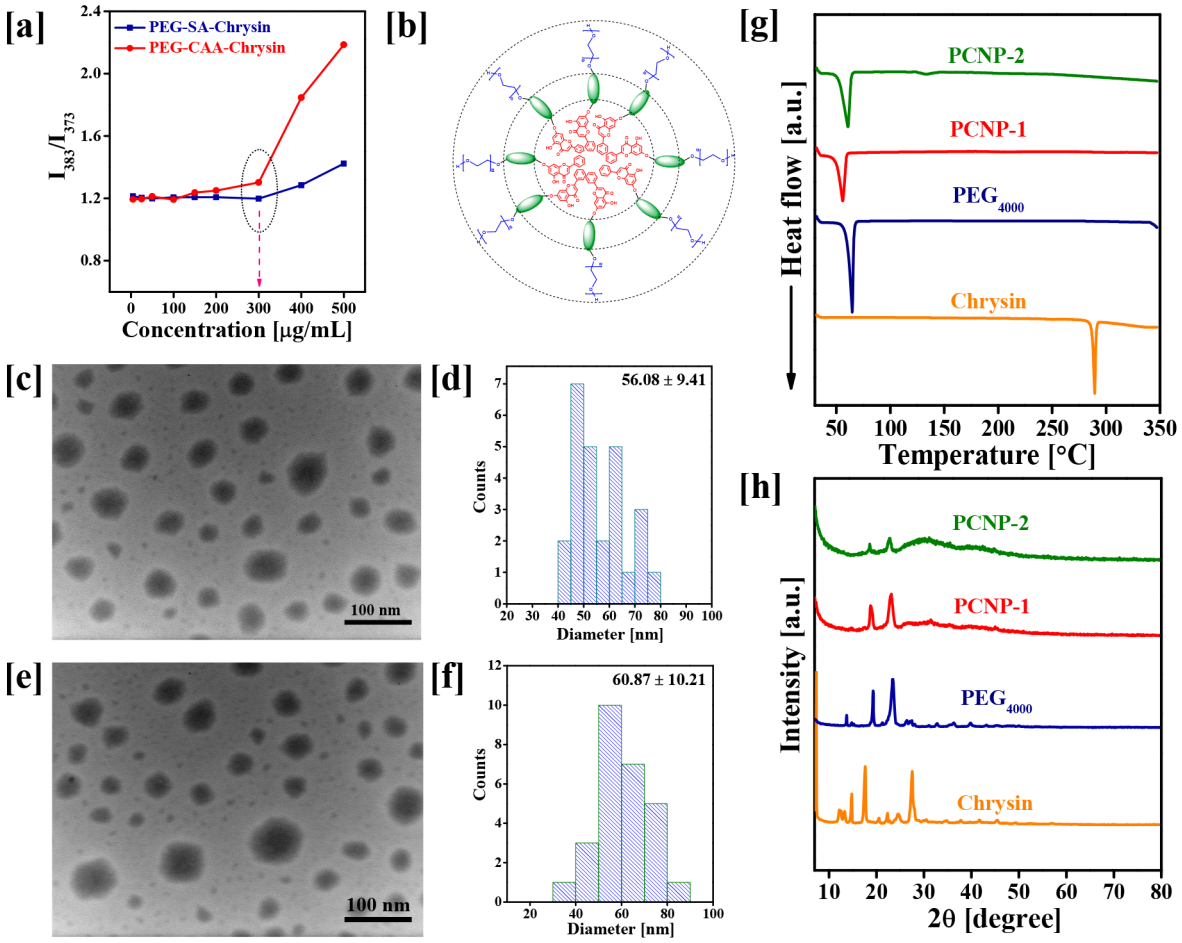

Figure 2. Characterization of PEGylated chrysin nanoparticles (PCNPs): (a) critical micelle concentration of different PEGylated chrysin conjugates; (b) a predictive model of PCNP formation; (c) TEM image and (d) particle size distribution histogram of succinoyl linkage containing PCNP (PCNP-1); (e) TEM image and (f) particle size distribution histogram of *cis*-aconityl linkage containing PCNP (PCNP-2); (g) DSC spectra of pure chrysin, PEG_{4000}, PCNP-1 and PCNP-2; and (h) XRD patterns of pure chrysin, PEG_{4000}, PCNP-1, and PCNP-2.

expressed as the mean ± standard deviation (SD). A *p*-value less than 0.05 was considered statistically significant.

3. RESULTS AND DISCUSSION

3.1. Synthesis and Characterizations of pH-Sensitive PEGylated Chrysin Conjugate. The synthesis procedure of PEGylated chrysin conjugate is schematically shown in Figure S1. These amphiphilic conjugates of chrysin were prepared by a two-step reaction. In the first step, the PEG_{4000} was reacted to succinoyl and *cis*-aconityl linkers via ring-opening mechanism. In the second step, chrysin was conjugated to succinoyl−PEG_{4000} or *cis*-aconityl−PEG_{4000} conjugates through esterification. The formation of the PEGylated chrysin conjugates was confirmed by ^{1}H NMR and FTIR techniques. Figure S2 shows the ^{1}H NMR spectra of PEG_{4000}, PEG_{4000}−SA, and PEG_{4000}−CAA where PEG_{4000} shows the characteristic chemical shift values at 3.65−3.68 and 4.26 ppm due to CH_2−CH_2 and −OH groups, respectively.[41] The chemical shift value observed at 2.64 ppm confirmed the formation of succinoyl−PEG_{4000}, while the peaks observed at 2.10 and 5.31 ppm confirmed the formation of *cis*-aconityl−PEG_{4000}. The pure chrysin shows the characteristic peaks at 6.20−6.22 ppm (6H), 6.41 ppm (8H), 6.57−6.59 ppm (3H), 7.48−7.49 ppm (4′H), 7.56 ppm (3′ and 5′H), 7.84 ppm (2′ and 6′H), 10.26 ppm (7OH), and 12.65 ppm (5OH)[21,42] (Figure S3). The ^{1}H NMR of a succinoyl linkage containing PEGylated chrysin shows the peaks of both PEG and chrysin. The peak observed at 3.65 ppm was due to −CH_2 of the PEG chain while the peaks corresponding to the protons of chrysin appeared at 6.35−6.52 ppm (6H and 8H), 6.56−6.63 ppm (3H), 7.51−7.89 ppm (2′, 3′, 5′ and 6′H), and 8.22−12.70 ppm (5H and 7OH) (Figure 1).

Similarly, the synthesis of *cis*-aconityl linkage containing PEGylated chrysin conjugate was confirmed by peaks observed at 3.65 ppm due to −CH_2 of the PEG chain and 6.38−6.54 ppm (6H and 8H), 6.65 ppm (3H), 7.53−7.90 ppm (2′, 3′, 5′ and 6′H), and 12.70 ppm (7OH) of chrysin. In FTIR analysis, pure PEG_{4000} shows characteristic peaks at 3456 cm^{-1} (−OH stretching), 2829 cm^{-1} (C−H stretching), 1286−1112 cm^{-1} (C−O stretching), and 951 and 844 cm^{-1} (C−O bending).[43] The FTIR peaks observed at 1736 cm^{-1} confirmed the formation of PEG_{4000}−SA while the peaks at 1964, 1576, and 1467 cm^{-1} confirmed the formation of PEG_{4000}−CAA. The pure chrysin molecule shows the characteristic peaks at 2727−2633 cm^{-1} (C−H stretching), 1650−1606 cm^{-1} (>C═O stretching), 1573−1446 cm^{-1} (C═C stretching), and 1164−1032 cm^{-1} (C−O−C stretching).[44] The succinoyl linkage containing PEGylated chrysin was confirmed by observed

https://doi.org/10.1021/acsomega.2c01041
ACS Omega 2022, 7, 15919−15928

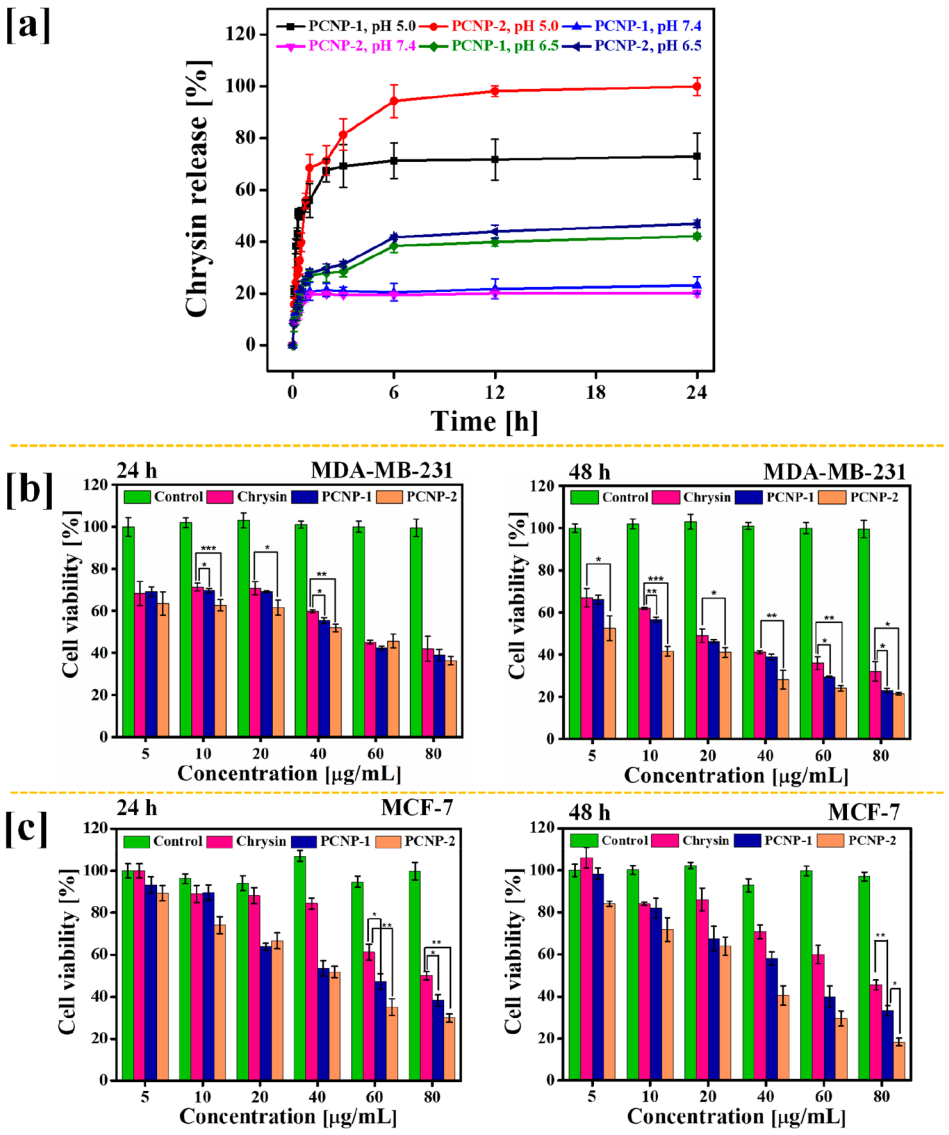

Figure 3. (a) Chrysin release patterns of succinoyl linkage containing PCNP (PCNP-1) and *cis*-aconityl linkage containing PCNP (PCNP-2) in sodium acetate buffer pH 5.0, phosphate buffer pH 6.5, and phosphate buffer saline pH 7.4. (b) Anticancer activity of pure chrysin, PCNP-1, and PCNP-2 against MDA-MB-231 cells after 24 and 48 h of treatment (*$p < 0.05$, **$p < 0.01$, ***$p < 0.001$). (c) Anticancer activity of pure chrysin, PCNP-1, and PCNP-2 against MCF-7 cells after 24 and 48 h of treatment (*$p < 0.05$, **$p < 0.01$).

FTIR peaks at 2881 cm^{-1} (C−H stretching of PEG), 1734−1646 cm^{-1} (>C═O stretching of ester bond and chrysin), 1569−1464 cm^{-1} (C═C stretching of chrysin), and 1144−1062 cm^{-1} (C−O−C stretching of chrysin and PEG). Similarly, the *cis*-aconityl linkage PEGylated chrysin conjugate shows the peaks at 2881 cm^{-1} (C−H stretching of PEG), 1733−1651 cm^{-1} (>C═O stretching of ester bond and chrysin), 1562−1469 cm^{-1} (C═C stretching of chrysin), and 1149−1060 cm^{-1} (C−O−C stretching of chrysin and PEG) (Figure S4). The UV−vis spectra of both PEGylated chrysin conjugates exhibited a shift in λ_{max} of chrysin (Figure S5). The observed λ_{max} for chrysin, PEG_{4000}−SA−CHRY, and PEG_{4000}−CAA−CHRY was 266, 279, and 285 nm, respectively.

3.2. Physicochemical Characterization of PEGylated Chrysin Nanoparticles. Critical micelle concentrations (CMC) of prepared PEG_{4000}−chrysin conjugates are shown in Figure 2a. The ratio of fluorescence intensities at 383 and 373 nm (I_{383}/I_{373}) was plotted against the concentration of conjugates to determine their CMC values. The fluorescence intensity increased suddenly and sharply at a concentration of 300 μg/mL of the conjugates, indicating the formation of micelles by the PEG_{4000}−chrysin conjugates. The same CMC values of both conjugates suggested that there was no significant role of linkers in the formation of PEGylated nanoparticles. Therefore, the observed results also depict the role of PEG_{4000} in the formation of stable and compact nanoparticles of chrysin. Figure 2b shows the predictive model representing a possible arrangement of chrysin, linkers, and PEG_{4000} molecules in self-assembled PCNP formed by PEG_{4000}−chrysin conjugates. The observed chrysin content was found to be 4.05% and 4.11% in PCNP-1 and PCNP-2, respectively (Figure S6). The TEM images and particle size distribution of PCNP-1 (Figure 2c,d) and PCNP-2 (Figure 2e,f) show the formation of spherical nanoparticles with a particle size of about 60 nm. The hydrodynamic diameter and surface charge of nanoparticles were measured by DLS

https://doi.org/10.1021/acsomega.2c01041
ACS Omega 2022, 7, 15919−15928

technique (Figure S7). The particle size, polydispersity index, and zeta potential values were 77.3 nm, 0.173 ± 0.003, and −4.25 mV for PCNP-1 and 75.5 nm, 0.185 ± 0.040, and −3.47 mV for PCNP-2, respectively. These results suggested the formation of nanosized and monodisperse particles.

The thermal behavior and physical state of chrysin after formation of the PCNPs were confirmed by DSC and XRD analysis. Figure 2g shows the DSC scans of chrysin, PEG_{4000}, PCNP-1, and PCNP-2. The pure chrysin shows a sharp endothermic peak at 289 °C[45] while pure PEG_{4000} shows an endothermic peak at 64 °C, corresponding to their melting points. The PCNP-1 and PCNP-2 show endothermic peaks at 55 and 59 °C, respectively, because of the presence of PEG_{4000}. However, the typical endothermic peak of pure chrysin was not observed in the scans of both PCNP-1 and PCNP-2, which specifies the phase conversion of chrysin. This change in the physical state of chrysin was further confirmed by PXRD analysis (Figure 2h). The XRD pattern of pure chrysin shows sharp peaks at 2θ values 7.2°, 12.2°, 13.2°, 14.7°, 17.5°, 20.3°, 22.3°, 24.6°, and 27.4° because of the crystalline nature of chrysin.[45] The pure PEG_{4000} shows three peaks at 2θ values 13.8°, 19.2°, and 23.3°. The PCNP-1 and PCNP-2 show the 2θ values at 18.8° and 23.05°, and 18.4° and 22.7°, respectively. So, because no sharp peaks of pure chrysin were observed in the XRD spectra of PCNP-1 and PCNP-2, the formation of amorphous nanoparticles was confirmed.[35]

3.3. PCNP Releases Chrysin in a pH-Dependent Manner. To evaluate the effect of succinoyl and *cis*-aconityl linkers on the release of chrysin from PCNPs, PCNP-1 and PCNP-2 were put into dialysis bags and dialyzed against SAB (pH 5.0), PB (pH 6.5), and PBS (pH 7.4). As shown in Figure 3a, the amount of chrysin released from PCNP-1 and PCNP-2 was 23.18 and 20.18%, respectively, after 24 h at pH 7.4. The chrysin release was 42.13% and 46.98% from PCNP-1 and PCNP-2, respectively, at pH 6.5. Hence, at the slightly acidic pH of the tumor microenvironment, the amount of chrysin released was higher than at the physiological pH 7.4. However, the chrysin release was about 60% in the first 3 h at pH 5.0 from both PCNP-1 and PCNP-2. Further, more than 90% of chrysin was released from PCNP-2 at pH 5.0 in 24 h, while 72.9% of chrysin was released from PCNP-1. As expected, a higher release of chrysin was observed at the lower pH 5.0 while a slow chrysin release was observed at pH 7.4. However, at pH 5.0 the accelerated chrysin release was observed because of the rapid hydrolysis of *cis*-aconityl linker. Hence, the observed results from this study suggest the effect of the pH-responsive (*cis*-aconityl) linker on the release of chrysin from the prepared PCNP-2 nanoparticles. Importantly, no burst release of drug was observed at pH 6.5 and pH 7.4 from either PCNP-1 or PCNP-2. Therefore, this pH-sensitive response of PCNP-2 may help in the site-specific release and delivery of chrysin.

3.4. Stability of PCNP. In order to check the stability of PCNP, particle size and drug content were measured at freeze temperature. Figure S8 shows the stability results of PCNP-1 and PCNP-2. Initially the particle sizes were observed as 77 and 75 nm for PCNP-1 and PCNP-2, respectively. After a period of 96 h, the particle sizes were observed as 91 and 78 nm for PCNP-1 and PCNP-2, respectively. Hence, no significant particle size changes were observed for either PCNP, which confers physical stability of the nanoparticles. Similarly, % chrysin content was observed as 91 and 98% over the period of 96 h. Hence, the observed physical as well as chemical stability results clearly confers the stability of the prepared PEGylated nanoparticles.

3.5. PCNP Causes Concentration- and Time-Dependent Cytotoxicities for Human Breast Cancer Cells. The cytotoxicity of prepared PCNP was evaluated against MCF-7 and MDA-MB-231 human breast cancer cells. The results of cell viability after treatment with chrysin, PCNP-1, and PCNP-2 at concentrations of 5, 10, 20, 40, 60, 80, and 100 μg/mL are presented in Figure 3b. It was observed that the PCNP-1 and PCNP-2 showed a significant decrease in the viability of breast cancer cells compared to chrysin in both dose- and time-dependent manner. In addition, PCNP-2 showed a higher inhibitory effect (p value < 0.05) as compared with PCNP-1 or chrysin after 24 and 48 h. The half-maximal inhibitory concentration (IC_{50}) of the pure chrysin, PCNP-1, and PCNP-2 after 24 and 48 h incubation time are presented in Table 1. The IC_{50} values (at 24 h) were found to be 52.2, 49.6, and 34.8 μg/mL for pure chrysin, PCNP-1, and PCNP-2, respectively. After 48 h, the IC_{50} values were decreased to 19.4, 15.2, and 6.2 μg/mL for pure chrysin, PCNP-1 and PCNP-2, respectively. In the case of MCF-7 cells, the IC_{50} values were 89.2, 48.3, and 35.7 μg/mL after 24 h of incubation with chrysin, PCNP-1, and PCNP-2, respectively (Figure 3c). The IC_{50} values were decreased after 48 h of incubation and observed to be 68.4, 44, and 26.1 μg/mL for chrysin, PCNP-1, and PCNP-2, respectively. The results of the cytotoxicity studies depict the potent and significantly enhanced anticancer activity of chrysin-conjugated nanoparticles in comparison to pure chrysin. The values of IC_{50} also suggest that PCNP-2 had comparatively higher cytotoxicity than PCNP-1.

Table 1. IC_{50} (μg/mL) Values for Prepared PCNPs[a]

time	chrysin	PCNP-1	PCNP-2
		MDA-MB-231	
24 h	52.2 ± 1.4	49.6 ± 4.5	34.8 ± 3.8$^{*,\#}$
48 h	19.4 ± 1.3	15.2 ± 0.7*	6.2 ± 2.3$^{***,\#\#}$
		MCF-7	
24 h	89.2 ± 10.8	48.3 ± 1.6**	35.7 ± 0.5$^{***,\#}$
48 h	68.4 ± 3.7	44.0 ± 1.3**	26.1 ± 3.5$^{***,\#\#}$

[a]Comparisons with chrysin are denoted with an asterisk (*) symbol while comparisons between PCNP-1 and PCNP-2 are denoted with a hash (#) symbol. Data are the mean ± SD of three replicates. $^{*}p < 0.05$, $^{**}p < 0.01$, $^{***}p < 0.001$, $^{\#}p < 0.05$, $^{\#\#}p < 0.01$, $^{\#\#\#}p < 0.001$.

3.6. Induction of Apoptosis by PCNP. Cytotoxicity of prepared PCNP was further confirmed by an apoptosis induction assay using AO/EtBr staining. This assay helps to check the changes at the cellular level and to differentiate between apoptotic, necrotic, and live cells after treatment with pure chrysin, PCNP-1, and PCNP-2. The AO dye gives green fluorescence after staining the nuclei of the live cells that have an intact cellular membrane, whereas EtBr emits red fluorescence after staining the nuclei of dead cells that have a compromised/damaged cellular membrane. Figure 4 represents the fluorescent images of MDA-MB-231 cells treated with 10 μg/mL concentration of pure chrysin, PCNP-1, and PCNP-2. After 24 h of incubation, MDA-MB-231 cells treated with pure chrysin did not show any significant signs of apoptosis and necrosis.

After 48 h, the cells started to emit red fluorescence that implies chrysin exhibited cell death after 48 h. However, cells treated with PCNP-1 and PCNP-2 showed apoptosis and

https://doi.org/10.1021/acsomega.2c01041
ACS Omega 2022, 7, 15919−15928

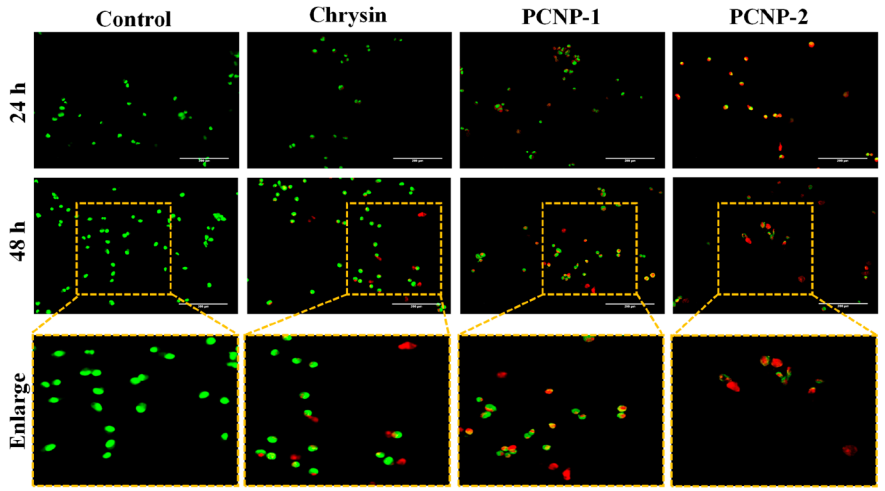

Figure 4. Apoptotic study by AO/EtBr staining: effect of pure chrysin, PCNP-1, and PCNP-2 on apoptosis induction in MDA-MB-231 cells. Cells were treated with 10 μg/mL of pure chrysin, PCNP-1, and PCNP-2 for 24 and 48 h. Images were captured by a fluorescence microscope. Scale bar = 200 μm.

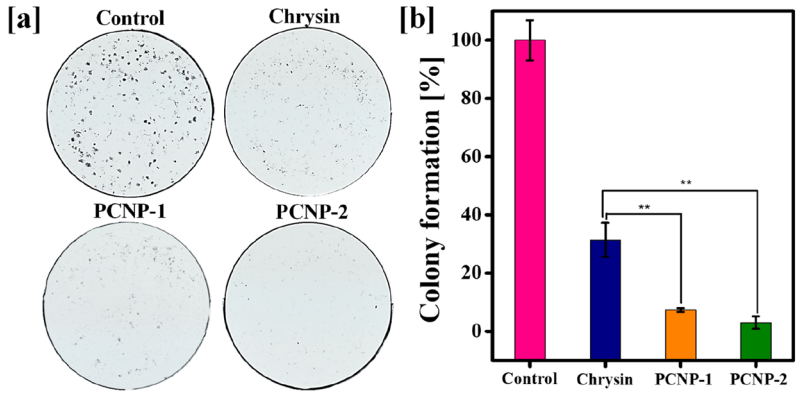

Figure 5. (a) The effect of pure chrysin, PCNP-1, and PCNP-2 on colony formation inhibition assay in MDA-MB-231 human breast cancer cells treated with 10 μg/mL for 24 h. (b) Quantitative assessment of colony formation experiments. (**$p < 0.01$).

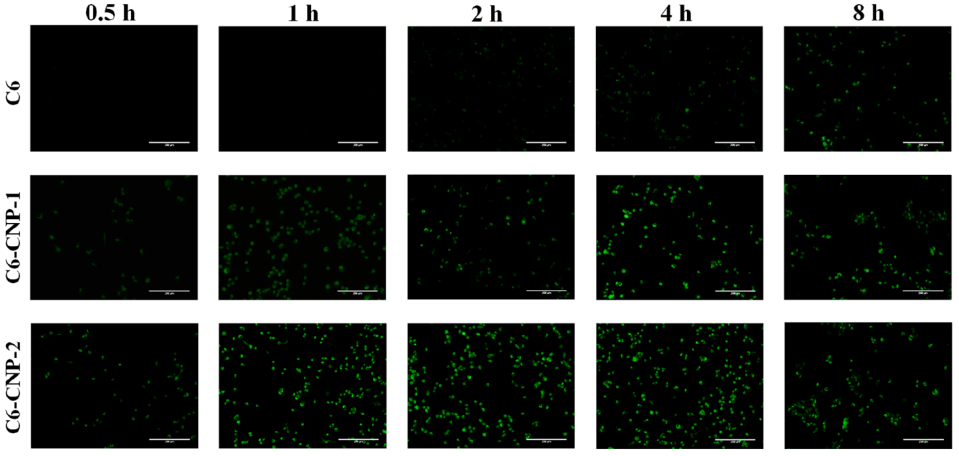

Figure 6. Cellular uptake of coumarin-6 (C6), C6-loaded PCNP-1 (C6-PCNP-1), and C6-loaded PCNP-2 (C6-PCNP-2) in MDA-MB-231 cells after different time intervals. Scale bar = 200 μm.

necrosis after 24 h, which were further increased after 48 h of incubation. The number of cell deaths was higher for PCNP-2 than PCNP-1 or pure chrysin at 10 μg/mL after the 24 and 48 h periods of time. The viable, apoptotic, and necrotic cells were also counted for each group represented in Figure S9. More than 95% of the control cells produced green fluorescent, implying healthy cells. The number of apoptotic and necrotic cells were observed higher for PCNP-2 (33.02 and 62.99%) as compared with PCNP-1 (29.45 and 48.93%) and chrysin (17.92 and 28.85%) after 48 h. The AO/EtBr staining results

https://doi.org/10.1021/acsomega.2c01041
ACS Omega 2022, 7, 15919−15928

revealed that PCNP-1 and PCNP-2 can induce apoptosis in a time-dependent manner in MDA-MB-231 cells, which also corroborates the results of the *in vitro* cytotoxicity assay. Therefore, these findings suggest that prepared PCNP have higher anticancer activity and can induce more apoptosis in MDA-MB-231 cells as compared with pure chrysin.

3.7. Colony Formation Assay. To further validate the cytotoxicity and growth inhibitory effects of chrysin and PCNP, the clonogenic assay was performed. As shown in Figure 5, with a 10 μg/mL concentration of chrysin, PCNP-1, and PCNP-2, the number of colony formations by MDA-MB-231 cells was decreased as compared with untreated control cells. Quantitatively, the colony formation activity of cells was observed to be 31.4%, 7.3%, and 2.9% after incubation with chrysin, PCNP-1, and PCNP-2, respectively. Further, the cells treated with PCNP-1 and PCNP-2 showed fewer colonies in comparison with the cells treated with pure chrysin. Following the patterns observed in the cytotoxicity assay and apoptosis study, PCNP-2 also showed more inhibition than PCNP-1 of colony formation by MDA-MB-231 cells.

3.8. Uptake of PCNP-1 and PCNP-2 by MDA-MB-231 Cells. To determine the uptake of the prepared PCNP-1 and PCNP-2 by MDA-MB-231 cells, PCNP-1 loaded with coumarin-6 (C6-PCNP-1) and PCNP-2 loaded with coumarin-6 (C6-PCNP-2) were prepared. Figure 6 shows the fluorescent images of MDA-MB-231 cells after treatment with native C6, C6-PCNP-1, and C6-PCNP-2 at 0.5, 1, 2, 4, and 8 h time intervals. Cells treated with C6-PCNP-1 and C6-PCNP-2 showed higher fluorescent intensity compared with native C6, suggesting that prepared nanoparticles were taken up more than hydrophobic C6. Further, it was found that the uptake of C6-PCNP-2 was faster and higher than the uptake of C6-PCNP-1. The results suggest that the synthesized PCNP could enhance the delivery of hydrophobic chrysin. Thus, increased delivery of chrysin could be responsible for the enhancement of anticancer activity and apoptosis of PCNP-1 and PCNP-2 against MDA-MB-231 cells.

4. CONCLUSION

In the present work, pH-sensitive PEGylated chrysin nanoparticles (PCNPs) were prepared and evaluated for their anticancer activity against MDA-MB-231 human breast cancer cells. The conjugation of chrysin with PEG via different pH-sensitive groups was confirmed by FTIR and ^{1}H NMR analysis. The prepared conjugates were self-assembled into nanoparticles with a particle size of about 60 nm. Both the PCNPs showed a pH-dependent drug release, that is, a faster and more complete drug release at acidic pH than physiological pH. The PCNPs with *cis*-aconityl linkage showed higher toxicity toward MDA-MB-231 cells as compared with pure chrysin or succinoyl linked PCNPs. Further, these PCNPs caused induction of apoptosis and a decrease in the colony formation ability of breast cancer cells. Therefore, this study highlights the development and significance of PEGylated chrysin as an anticancer agent.

ASSOCIATED CONTENT

Supporting Information

The Supporting Information is available free of charge at https://pubs.acs.org/doi/10.1021/acsomega.2c01041.

Reaction schemes representing the PEGylation of chrysin; ^{1}H NMR, FTIR, and UV−visible spectra of chrysin and PEGylated chrysin conjugates; chemical structure of chrysin; particle size distribution of PCNP-1 and PCNP-2; stability results of the PEGylated chrysin nanoparticles; and percentage of viable, early apoptotic, late apoptotic, and necrotic cells after the treatment with chrysin, PCNP-1, and PCNP-2 for 24 and 48 h (PDF)

AUTHOR INFORMATION

Corresponding Authors

Hitesh Kulhari − *School of Nano Sciences, Central University of Gujarat, Gandhinagar 382030, India; Department of Pharmaceutical Technology (Formulations), National Institute of Pharmaceutical Education and Research, Guwahati, Assam 781101, India;* orcid.org/0000-0002-1834-1132; Email: hitesh.kulhari@cug.ac.in

Deep Pooja − *School of Pharmacy, National Forensic Sciences University, Gandhinagar, Gujarat 382007, India;* Email: d.dpooja00@gmail.com

Authors

Ashok Kumar Jangid − *School of Nano Sciences, Central University of Gujarat, Gandhinagar 382030, India*

Raghu Solanki − *School of Life Sciences, Central University of Gujarat, Gandhinagar 382030, India*

Sunita Patel − *School of Life Sciences, Central University of Gujarat, Gandhinagar 382030, India*

Kanakaraju Medicherla − *Department of Human Genetics, College of Science and Technology, Andhra University, Visakhapatnam 530003, India*

Complete contact information is available at: https://pubs.acs.org/10.1021/acsomega.2c01041

Notes

The authors declare no competing financial interest.

ACKNOWLEDGMENTS

The authors thank the Central University of Gujarat, Gandhinagar and the National Forensic Sciences University, Gandhinagar for providing the necessary facilities and support. The authors acknowledge Central Instrumentation Facilities, Central University of Gujarat, Gandhinagar for the characterization of samples. H.K. acknowledges the Department of Science and Technology (DST), New Delhi for an INSPIRE Faculty Award and DST-SERB, New Delhi for the ECR award. A.K.J. acknowledges SERB, DST, New Delhi for providing a Research Fellowship. R.S. acknowledges the Council of Scientific and Industrial Research, New Delhi for a Senior Research Fellowship.

ABBREVIATIONS

PEG, polyethylene glycol; PCNP-1, PEG_{4000}−chrysin via succinoyl linker nanoparticles; PCNP-2, PEG_{4000}−chrysin via *cis*-aconityl linker nanoparticles; C6, coumarin-6; DMAP, 4-dimethylaminopyridine; CAA, *cis*-aconitic anhydride; EDC, 1-ethyl-3-(3-(dimethylamino)propyl) carbodiimide; HOBt, hydroxybenzotriazole; FBS, fetal bovine serum; DMSO, dimethyl sulfoxide; PBS, phosphate buffer saline; ^{1}H NMR, nuclear magnetic resonance; FTIR, Fourier transform infrared

https://doi.org/10.1021/acsomega.2c01041
ACS Omega 2022, 7, 15919−15928

REFERENCES

(1) Lagoa, R.; Silva, J.; Rodrigues, J. R.; Bishayee, A. Advances in Phytochemical Delivery Systems for Improved Anticancer Activity. *Biotechnol. Adv.* **2020**, *38*, 107382.

(2) Maruhashi, R.; Eguchi, H.; Akizuki, R.; Hamada, S.; Furuta, T.; Matsunaga, T.; Endo, S.; Ichihara, K.; Ikari, A. Chrysin Enhances Anticancer Drug-Induced Toxicity Mediated by the Reduction of Claudin-1 and 11 Expression in a Spheroid Culture Model of Lung Squamous Cell Carcinoma Cells. *Sci. Rep.* **2019**, *9* (1), 13753.

(3) Halevas, E.; Mavroidi, B.; Antonoglou, O.; Hatzidimitriou, A.; Sagnou, M.; Pantazaki, A. A.; Litsardakis, G.; Pelecanou, M. Structurally Characterized Gallium-Chrysin Complexes with Anticancer Potential. *Dalton Transactions* **2020**, *49* (8), 2734−2746.

(4) Rasouli, S.; Montazeri, M.; Mashayekhi, S.; Sadeghi-Soureh, S.; Dadashpour, M.; Mousazadeh, H.; Nobakht, A.; Zarghami, N.; Pilehvar-Soltanahmadi, Y. Synergistic Anticancer Effects of Electrospun Nanofiber-Mediated Codelivery of Curcumin and Chrysin: Possible Application in Prevention of Breast Cancer Local Recurrence. *J. Drug Deliv Sci. Technol.* **2020**, *55*, 101402.

(5) Kasala, E. R.; Bodduluru, L. N.; Madana, R. M.; V, A. K.; Gogoi, R.; Barua, C. C. Chemopreventive and Therapeutic Potential of Chrysin in Cancer: Mechanistic Perspectives. *Toxicol. Lett.* **2015**, *233* (2), 214−225.

(6) Khoo, B. Y.; Chua, S. L.; Balaram, P. Apoptotic Effects of Chrysin in Human Cancer Cell Lines. *Int. J. Mol. Sci.* **2010**, *11* (5), 2188−99.

(7) Xu, Y.; Tong, Y.; Ying, J.; Lei, Z.; Wan, L.; Zhu, X.; Ye, F.; Mao, P.; Wu, X.; Pan, R.; et al. Chrysin Induces Cell Growth Arrest, Apoptosis, and ER Stress and Inhibits the Activation of STAT3 through the Generation of ROS in Bladder Cancer Cells. *Oncol. Lett.* **2018**, *15* (6), 9117−9125.

(8) Song, H.-Y.; Kim, H.-M.; Mushtaq, S.; Kim, W. S.; Kim, Y. J.; Lim, S.-T.; Byun, E.-B. Gamma-Irradiated Chrysin Improves Anticancer Activity in HT-29 Colon Cancer Cells Through Mitochondria-Related Pathway. *J. of Med. Food.* **2019**, *22* (7), 713−721.

(9) Samarghandian, S.; Azimi-Nezhad, M.; Borji, A.; Hasanzadeh, M.; Jabbari, F.; Farkhondeh, T.; Samini, M. Inhibitory and Cytotoxic Activities of Chrysin on Human Breast Adenocarcinoma Cells by Induction of Apoptosis. *Pharmacogn. Mag.* **2016**, *12* (47), 436−440.

(10) Lee, S. H.; Lee, Y.-S.; Song, J. G.; Han, H.-K. Improved In Vivo Effect of Chrysin as an Absorption Enhancer Via the Preparation of Ternary Solid Dispersion with Brij®L4 and Aminoclay. *Cur. drug deliv.* **2018**, *16* (1), 86−92.

(11) Walle, T.; Otake, Y.; Brubaker, J. A.; Walle, U. K.; Halushka, P. V. Disposition and Metabolism of the Flavonoid Chrysin in Normal Volunteers. *Br. J. Clin. Pharmacol.* **2001**, *51* (2), 143−146.

(12) Kumar, R.; Thakur, A. K.; Chaudhari, P.; Banerjee, N. Particle Size Reduction Techniques of Pharmaceutical Compounds for the Enhancement of Their Dissolution Rate and Bioavailability. *J. Pharm. Innov.* **2021**, DOI: 10.1007/s12247-020-09530-5.

(13) Dong, D.; Quan, E.; Yuan, X.; Xie, Q.; Li, Z.; Wu, B. Sodium Oleate-Based Nanoemulsion Enhances Oral Absorption of Chrysin through Inhibition of UGT-Mediated Metabolism. *Mol. Pharma.* **2017**, *14* (9), 2864−2874.

(14) Ghamkhari, A.; Pouyafar, A.; Salehi, R.; Rahbarghazi, R. Chrysin and Docetaxel Loaded Biodegradable Micelle for Combination Chemotherapy of Cancer Stem Cell. *Pharm. Res.* **2019**, *36* (12), 165.

(15) Fenyvesi, F.; Nguyen, T. L.; Haimhoffer, Á.; Rusznyák, Á.; Vasvári, G.; Bácskay, I.; Vecsernyés, M.; Ignat, S.-R.; Dinescu, S.; Costache, M.; et al. Cyclodextrin Complexation Improves the Solubility and Caco-2 Permeability of Chrysin. *Materials* **2020**, *13* (16), 3618.

(16) Sa, R.; Zhang, Y.; Deng, Y.; Huang, Y.; Zhang, M.; Lou, B. Novel Salt Cocrystal of Chrysin with Berberine: Preparation, Characterization, and Oral Bioavailability. *Cryst. Growth & Des.* **2018**, *18* (8), 4724−4730.

(17) Zheng, X.; Meng, W.-D.; Xu, Y.-Y.; Cao, J.-G.; Qing, F.-L. Synthesis and Anticancer Effect of Chrysin Derivatives. *Bioorg. Med. Chem. Lett.* **2003**, *13* (5), 881−884.

(18) Huang, X.; Liao, W.; Xie, Z.; Chen, D.; Zhang, C. Y. A PH-Responsive Prodrug Delivery System Self-Assembled from Acid-Labile Doxorubicin-Conjugated Amphiphilic PH-Sensitive Block Copolymers. *Mater. Sci. Eng. C* **2018**, *90*, 27−37.

(19) Anari, E.; Akbarzadeh, A.; Zarghami, N. Chrysin-Loaded PLGA-PEG Nanoparticles Designed for Enhanced Effect on the Breast Cancer Cell Line. *Artif. Cells, Nanomed., and Biotechnol.* **2016**, *44* (6), 1410−1416.

(20) Mohammadian, F.; Abhari, A.; Dariushnejad, H.; Nikanfar, A.; Pilehvar-Soltanahmadi, Y.; Zarghami, N. Effects of Chrysin-PLGA-PEG Nanoparticles on Proliferation and Gene Expression of MiRNAs in Gastric Cancer Cell Line. *Iran J. Cancer Prev.* **2016**, *9* (4), No. e4190.

(21) Zheng, H.; Li, S.; Pu, Y.; Lai, Y.; He, B.; Gu, Z. Nanoparticles Generated by PEG-Chrysin Conjugates for Efficient Anticancer Drug Delivery. *Euro. J. of Pharm. and Biopharm.* **2014**, *87* (3), 454−460.

(22) Chandel, A. K. S.; Kumar, C. U.; Jewrajka, S. K. Effect of Polyethylene Glycol on Properties and Drug Encapsulation−Release Performance of Biodegradable/Cytocompatible Agarose−Polyethylene Glycol−Polycaprolactone Amphiphilic Co-Network Gels. *ACS Appl. Mater. & Inter.* **2016**, *8* (5), 3182−3192.

(23) Yadav, N.; Kumar, N.; Prasad, P.; Shirbhate, S.; Sehrawat, S.; Lochab, B. Stable Dispersions of Covalently Tethered Polymer Improved Graphene Oxide Nanoconjugates as an Effective Vector for SiRNA Delivery. *ACS Appl. Bio Mater.* **2018**, *10* (17), 14577−14593.

(24) Yadav, N.; Kannan, D.; Patil, S.; Singh, S.; Lochab, B. Amplified Activity of Artesunate Mediated by Iron Oxide Nanoparticles Loaded on a Graphene Oxide Carrier for Cancer Therapeutics. *ACS Appl. Bio Mater.* **2020**, 3 (10), 6722−6736.

(25) Pei, X.; Zhu, Z.; Gan, Z.; Chen, J.; Zhang, X.; Cheng, X.; Wan, Q.; Wang, J. PEGylated Nano-Graphene Oxide as a Nanocarrier for Delivering Mixed Anticancer Drugs to Improve Anticancer Activity. *Sci. Rep.* **2020**, *10* (1), 2717.

(26) Debotton, N.; Dahan, A. Applications of Polymers as Pharmaceutical Excipients in Solid Oral Dosage Forms. *Med. Res. Rev.* **2017**, *37* (1), 52−97.

(27) Mishra, P.; Nayak, B.; Dey, R. K. PEGylation in Anti-Cancer Therapy: An Overview. *Asian J. Pharm. Sci.* **2016**, *11* (3), 337−348.

(28) Nguyen, A.; Ando, H.; Böttger, R.; DurgaRao Viswanadham, K. K.; Rouhollahi, E.; Ishida, T.; Li, S.-D. Utilization of Click Chemistry to Study the Effect of Poly(Ethylene)Glycol Molecular Weight on the Self-Assembly of PEGylated Gambogic Acid Nanoparticles for the Treatment of Rheumatoid Arthritis. *Biomat. Sci.* **2020**, *8* (16), 4626−4637.

(29) Prabhuraj, R. S.; Bomb, K.; Srivastava, R.; Bandyopadhyaya, R. Selection of Superior Targeting Ligands Using PEGylated PLGA Nanoparticles for Delivery of Curcumin in the Treatment of Triple-Negative Breast Cancer Cells. *J. of D. Deli. Sci. and Technol.* **2020**, *57*, 101722.

(30) Mu, J.; Zhong, H.; Zou, H.; Liu, T.; Yu, N.; Zhang, X.; Xu, Z.; Chen, Z.; Guo, S. Acid-Sensitive PEGylated Paclitaxel Prodrug Nanoparticles for Cancer Therapy: Effect of PEG Length on Antitumor Efficacy. *J. of Cont. Rel.* **2020**, *326* (July), 265−275.

(31) Phung, C. D.; Le, T. G.; Nguyen, V. H.; Vu, T. T.; Nguyen, H. Q.; Kim, J. O.; Yong, C. S.; Nguyen, C. N. PEGylated-Paclitaxel and Dihydroartemisinin Nanoparticles for Simultaneously Delivering Paclitaxel and Dihydroartemisinin to Colorectal Cancer. *Pharm. Res.* **2020**, *37* (7), 129.

(32) Wang, S.; Huang, P.; Chen, X. Stimuli-Responsive Programmed Specific Targeting in Nanomedicine. *ACS Nano* **2016**, *10* (3), 2991−2994.

(33) Simmons, J. K.; Burke, P. J.; Cochran, J. H.; Pittman, P. G.; Lyon, R. P. Reducing the Antigen-Independent Toxicity of Antibody-Drug Conjugates by Minimizing Their Non-Specific Clearance through PEGylation. *Toxicol. Appl. Pharmacol.* **2020**, *392*, 114932.

https://doi.org/10.1021/acsomega.2c01041
ACS Omega 2022, 7, 15919−15928

(34) Hsu, C.-W.; Hsieh, M.-H.; Xiao, M.-C.; Chou, Y.-H.; Wang, T.-H.; Chiang, W.-H. PH-Responsive Polymeric Micelles Self-Assembled from Benzoic-Imine-Containing Alkyl-Modified PEGylated Chitosan for Delivery of Amphiphilic Drugs. *Int. J. of Bio. Macromol.* **2020**, *163*, 1106−1116.
(35) Jangid, A. K.; Pooja, D.; Jain, P.; Rompicharla, S. V. K.; Ramesan, S.; Kulhari, H. A Nanoscale, Biocompatible and Amphiphilic Prodrug of Cabazitaxel with Improved Anticancer Efficacy against 3D Spheroids of Prostate Cancer Cells. *Mater. Adv.* **2020**, *1* (4), 738−748.
(36) Jangid, A. K.; Patel, K.; Jain, P.; Patel, S.; Gupta, N.; Pooja, D.; Kulhari, H. Inulin-Pluronic-Stearic Acid Based Double Folded Nanomicelles for PH-Responsive Delivery of Resveratrol. *Carb. Poly.* **2020**, *247*, 116730.
(37) Kulhari, H.; Pooja, D.; Shrivastava, S.; Kuncha, M.; Naidu, V. G. M.; Bansal, V.; Sistla, R.; Adams, D. J. Trastuzumab-Grafted PAMAM Dendrimers for the Selective Delivery of Anticancer Drugs to HER2-Positive Breast Cancer. *Sci. Rep.* **2016**, *6* (1), 23179.
(38) Solanki, R.; Patel, K.; Patel, S. Bovine Serum Albumin Nanoparticles for the Efficient Delivery of Berberine: Preparation, Characterization and In Vitro Biological Studies. *Colloids Surf., A Physicochem. Eng. Asp.* **2021**, *608*, 125501.
(39) Gui, K.; Zhang, X.; Chen, F.; Ge, Z.; Zhang, S.; Qi, X.; Sun, J.; Yu, Z. Lipid-Polymer Nanoparticles with CD133 Aptamers for Targeted Delivery of All-Trans Retinoic Acid to Osteosarcoma Initiating Cells. *Biomed & Pharmacother.* **2019**, *111*, 751−764.
(40) Kulhari, H.; Pooja, D.; Shrivastava, S.; Telukutala, S. R.; Barui, A. K.; Patra, C. R.; Naidu Vegi, G. M.; Adams, D. J.; Sistla, R. Cyclic-RGDfK Peptide Conjugated Succinoyl-TPGS Nanomicelles for Targeted Delivery of Docetaxel to Integrin Receptor over-Expressing Angiogenic Tumours. *Nanomed.: NBM.* **2015**, *11* (6), 1511−1520.
(41) Ye, W.; Zhao, Y.; Li, H.; Na, R.; Li, F.; Mei, Q.; Zhao, M.; Zhou, S. Doxorubicin-Poly (Ethylene Glycol)-Alendronate Self-Assembled Micelles for Targeted Therapy of Bone Metastatic Cancer. *Sci. Rep.* **2015**, *5* (1), 14614.
(42) Kulkarni, A. D.; Belgamwar, V. S. Inclusion Complex of Chrysin with Sulfobutyl Ether-β-Cyclodextrin (Captisol®): Preparation, Characterization, Molecular Modelling and in Vitro Anticancer Activity. *J. Mol. Struct.* **2017**, *1128*, 563−571.
(43) Altamimi, M. A.; Elzayat, E. M.; Qamar, W.; Alshehri, S. M.; Sherif, A. Y.; Haq, N.; Shakeel, F. Evaluation of the Bioavailability of Hydrocortisone When Prepared as Solid Dispersion. *Sau. Pharm. J.* **2019**, *27* (5), 629−636.
(44) Zhu, Z. Y.; Luo, Y.; Liu, Y.; Wang, X. T.; Liu, F.; Guo, M. Z.; Wang, Z.; Liu, A. J.; Zhang, Y. M. Inclusion of Chrysin in β-Cyclodextrin and Its Biological Activities. *J. of Drug Deli. Sci. and Technol.* **2016**, *31*, 176−186.
(45) Chadha, R.; Bhalla, Y.; Nandan, A.; Chadha, K.; Karan, M. Chrysin Cocrystals: Characterization and Evaluation. *J. of Pharma. and Biomed. Ana.* **2017**, *134*, 361−371.

https://doi.org/10.1021/acsomega.2c01041
ACS Omega 2022, 7, 15919−15928